Microchemical Journal 193 (2023) 109044

Contents lists available at ScienceDirect

Microchemical Journal

journal homepage: www.elsevier.com/locate/microc

A novel integrated platform enabling simultaneous microextraction and chemical analysis on-chip

Elia Santigosa-Murillo [a], Alexandre Moreno [b], María Ramos-Payán [c], Juan Manuel Ríos [b], Xavier Muñoz-Berbel [b,d], María Muñoz [a,*], Pablo Giménez-Gómez [b,1,*]

[a] Department of Analytical Chemistry, Universitat Autónoma de Barcelona, 08193 Bellaterra, Barcelona, Spain
[b] Instituto de Microelectrónica de Barcelona (IMB-CNM, CSIC), 08193 Bellaterra, Barcelona, Spain
[c] Department of Analytical Chemistry, Faculty of Chemistry, University of Seville, 41012 Seville, Spain
[d] CIBER de Bioingeniería, Biomateriales y Biomedicina (CIBER-BBN), Spain

ARTICLE INFO

Keywords:
Electromembrane microextraction
Electrochemical impedance spectroscopy detection
Biological, pharmaceutical or environmental analytes detection
Thin-film microelectrodes

ABSTRACT

The nature and size of biological, pharmaceutical or environmental analytes complicates their extraction and detection outside of laboratories and near the site of interest by the current chromatographic methods because they require the combination of bulky extraction and detection methods. In order to solve this inefficient centralized control, a ground-breaking and miniaturized proof of concept platform is developed in this work. The platform integrates for the very first time an electro-membrane extraction process and an accurate analyte quantification method in the same device, by using electrochemical impedance spectroscopy (EIS) as analytical technique. The microfluidic flow cell, including the microfluidic components, is fabricated in polymeric materials by rapid prototyping techniques. It comprises a four-electrode platinum thin-film chip that enables the control of the microextraction and the full characterization of the process, i.e., extraction efficiency determination, at the same time. The microfluidic system has been simulated by using computational tools, enabling an accurate prediction of the effect of the different experimental conditions in the microextraction efficiency. The platform has been validated in the microextraction of the nonsteroidal anti-inflammatory drug ketoprofen in a range from 0.5 ppm to 6 ppm. The predicted microextraction efficiency values obtained by EIS were compared with those calculated from the high-performance liquid chromatography coupled with a diode array detector (HPLC-DAD), showing an excellent agreement. This validates the high potential of this integrated and miniaturized platform for the simultaneous extraction by electro-membrane and also the analysis within the platform, solving one of the of most important limitations of current systems.

1. Introduction

Lab-on-a-chips (LOCs) implement multiple functions in a low-cost, miniaturised and automated system, widely improving the performance of traditional laboratory assays in portability and robustness [1]. They are simple-to-operate (even for non-trained personnel) and safe, minimizing the users' exposure to chemicals and human errors. Moreover, their low sample and reagents consumption reduces the waste production and the assay time, making them ideal for in-field analysis, and enabling the application of on-time corrective actions in very short times, a key factor in environmental control, clinical analysis or quality control in the food industry [2].

The sample processing and the analyte detection method are the key factors in miniaturized systems because of the complexity of real samples matrices [3]. For the sample processing, different microextraction techniques [4] have been adapted to microfluidic platforms to take advantage of the LOC functionalities, like the liquid phase microextraction (LPME) and the electromembrane extraction (EME). In LPME, the neutral analytes diffuse through a supported liquid membrane [5], while in the EME, the electric field generated between two electrodes placed on each of the liquid phases (the donor and the acceptor) allows the charged analytes to move from the donor to the acceptor phase [6]. Regarding the chemical analysis, there is an increasing demand on the ever-smaller portable analytical devices to monitor in a decentralised

* Corresponding authors.
E-mail addresses: maria.munoz@uab.cat (M. Muñoz), pablo.gimenez-gomez@mmk.su.se (P. Giménez-Gómez).
[1] Present address: Department of Materials and Environmental Chemistry, Stockholm University, 106 91Stockholm, Sweden.

https://doi.org/10.1016/j.microc.2023.109044
Received 28 April 2023; Received in revised form 28 June 2023; Accepted 30 June 2023
Available online 1 July 2023

manner (i.e., environmental monitoring, biochemical detection or clinical diagnostics [7–10]), without the need for sample collection and transport to the laboratory to speed-up the analysis and shorten decision-making at lower cost.

Such current trend towards the integration of microextraction and chemical analysis in a single LOC [11–13] began with the first molecular separation using microchannels proposed by Sato et al. in 2000 [14]. From there, many other microfluidic systems have been developed aiming to improve the low efficiency and reproducibility of this initial system. In 2010, the first EME-based microfluidic system integrating a supported liquid membrane and two platinum threads as electrodes in a polymethyl methacrylate (PMMA) platform was published [15]. Although it had high extraction efficiencies, its single-use design limited its applicability. After that, other systems coupled to HPLC-DAD have been developed with the aim of miniaturizing the channels used for the extraction of different biological, pharmaceutical or environmental analytes [16–18] to reduce the analysis time, but they had low enrichment factors, which did not allow to detect the very low concentrations required in environmental monitoring. In 2015, a new system improving the enrichment factor of the extraction with novel microchannel geometries and working in stationary conditions was developed [18], but the assay time and the processed sample volume was very high. At that time, the integration of LPME and EME in microfluidics allowed the simultaneous extraction of analytes of similar nature, but the selective microextraction of analytes of different nature was still a challenge to solve. In 2016, the first system trying to solve this challenge was proposed [19]. The system (working in continuous mode) integrated a LPME process into microfluidics, resulting in higher extraction efficiencies and enrichment factors. However, the technique did not allow a good extraction when using analytes with different structure, acid-basic nature and polarity. This limitation was solved by Yamini et al. [20] by connecting two miniaturised EME devices and by using an acceptor solution adjusted with two different pH to favour the selective analyte extraction. Although the extraction was good, the system required sample preconcentration to operate in stationary flow, consuming important sample volumes (1,0 mL) and requiring large extraction times (more than 40 min). During the last five years, the first microchips integrating LPME and EME [21] or EME-EME [22,23] for the separation of basic/acid analytes with high efficiency extraction (around 100 %) have been developed. These microchips-based devices can obtain reproducible results with high robustness and sensitivity in a miniaturized way, consuming very low volumes of reagents and samples. Moreover, the high miniaturisation enables to shorten the analysis time and improve the process efficiency. In addition, the mass transfer is enhanced by the use of microchannels, and the use of electrodes in EME microsystems allow selective microextraction by adjusting the direction and the magnitude of the power supply.

But, despite of the advantages mentioned above of microchips-based systems, all of the reported systems still require the combination of the device with traditional equipment for the chemical analysis (HPLC-DAD), limiting their fully portability and their on-line application for in situ analysis. At this point, electrochemical impedance spectroscopy (EIS) technique has demonstrated a high potential to characterize the solutions and the membrane integrated into non-miniaturised EME systems [24–26]. In 2020, the very first EME-based millifluidic device impedance characterization was validated [27] and applied to the extraction of parabens with very high efficiencies in urine samples (86%-92%), opening a new challenge to the monitoring of processes in real time. Nevertheless, this system used platinum threads as electrodes, and presented two important limitations: (1) the reproducibility and reusability of the system was very low; and (2) it did not work as a real multiplexed system for the simultaneous extraction and chemical analysis of the microsystem, limiting their potential application in decentralised assays.

To solve the current challenge of simultaneous microextraction and chemical analysis, a pioneering miniaturised microfluidic platform is studied and presented in this work as a proof of concept for the very first time. This proof-of-concept platform is fabricated by multi-layered PMMA and it integrated two silicon chips with four platinum microelectrodes placed face-to-face in the microchannels respectively immersed in the donor and in the acceptor solution. The multielectrode system enabled to properly study the option to use different areas and electrodes to evaluate the microextraction through chemical analysis of both phases and the membrane by EIS, meaning in a fully characterization and control of the process. The system has been fully studied by using computational software and EIS as characterization technique in terms of microfluidic design and microelectrodes configuration. The predicted microextraction efficiencies by ESI were compared to those obtained from the HPLC-DAD analysis. The microfluidic flow cell has been fully characterised to perfectly understand and control the microextraction process for the selective determination of the ketoprofen (KTP) [28,29], a non-steroidal anti-inflammatory drug, in a robust and reproducible way, obtaining promising results.

2. Experimental

2.1. Reagents and solutions

KTP, 1-octanol, formic acid, ammonium chloride, sodium phosphate dibasic, methanol and chloride acid, were purchased from Sigma–Aldrich (Madrid, Spain). All the solutions used in this work were prepared in deionizing water, except where otherwise noted. A stock methanol-based solution of 100 mg/L of KTP was prepared every week and stored at 4 °C in the fridge. For the assays, water-based solutions of KTP were prepared every day from this stock solution. To mechanically clean and electrochemically activate the microelectrodes, ethanol 96%, 6 M sulphuric acid and 0.1 M potassium nitrate were prepared and stored at room temperature.

2.2. Equipment

For HPLC-based separation, a liquid chromatograph (Agilent 1100 series, Barcelona, Spain) equipped with a binary pump system (G1312A, Agilent, Barcelona, Spain) and an autosampler injector (G1313A 5 μL, Agilent, Barcelona, Spain) was used. The set-up for the KTP analysis was completed with a column (LiChroCART1 75–4 Purosphere STAR RP-18e, 3 mm, 75 mm × 4.0 mm of inner diameter, VWR, Barcelona, Spain) preceded by a guard column (Kromasil1 100 Å, C18, 5 mm, 20 mm × 4.6 mm of inner diameter, Scharlab S.L., Barcelona, Spain).

To electrochemically activate the microelectrodes, an Autolab electrochemical workstation (PGSTAT-100 potentiostat–galvanostat, Ecochemie, Utrecht, The Netherlands) controlled with the NOVA advanced electrochemical software was used. The electrochemical cell (platinum microelectrodes were used as working electrodes) was completed with a commercial platinum electrode as counter electrode (Radiometer Analytical, Lyon, France) and a commercial Ag/AgCl (3 M KCl) double junction reference electrode (Orion 92–02-00, Thermo Fisher Scientific Inc., Beverly, USA).

Impedance measurements were performed with a 1260 Solartron Impedance Analyzer (Solartron Analytical, Farnborough, UK), controlled with the ZPlot® software.

The polymeric microfluidic flow cell was manufactured by using a CO_2 laser cutter (Epilog Mini 24, Epilog Laser, United States), followed by a solvent assisted bonding under pressure and temperature with a manual 2-column laboratory press (PW 10*H*-HKP300, Paul-Otto Weber GmbH, Remshalden, Germany).

2.3. Design and fabrication of the microfluidic flow cell

Silicon chips already developed by the group and applied to lactic and malic detection [30] were used in this case, which containing four independent in-parallel platinum (Pt) microelectrodes (i.e., one of 2 mm

× 2.5 mm and three of 1 mm × 2.5 mm, separated each other 0.6 mm). The chips also included four contact pads located 2.9 mm away from the microelectrodes to enable the electrical connection between the microelectrodes to the external equipment once implemented in the polymeric microfluidic flow cell for extraction and chemical analysis of analytes.

The microfluidic flow cell (30 mm × 30 mm × 11.25 mm) consisted of two symmetrical structures, each one containing three independent PMMA layers, which chemically bonded through a solvent-assisted process (7.5 kN, 80 °C) with methacrylic acid (Fig. 1A). The first layer (layer 1; 5 mm-thick) contained two 5 mm-diameter cylindrical holes for positioning the fitting threads working as fluidic inlet and outlet, which were connected to external Teflon tubes (0.5-mm inner diameter, Teknokroma, Barcelona, Spain). The layer 1 also contained a hole (9.4 mm × 2.5 mm) for embedding the spring-loader connector which enabled the electrical connection between the chip positioned in the other symmetrical structure and the external potentionstat-galvanostat. The second layer (layer 2; 500 μm-thick) contained a hole (11 mm × 9 mm × 0.5 mm) with the footprint of the silicon chip for its correct positioning and alignment with the spring-loaded connector and the microfluidic channels from the other PMMA layers. Besides, this layer contained two holes of 1 mm-diameter aligned with the fitting threads from layer 1, to ensure properly fluidic connection between layers (from the microfluidic channel in layer 3 to the inlet/outlet in layer 1). Finally, layer 3 defined the microfluidic channel (22 mm × 3 mm), which was aligned with the four platinum microelectrodes of the chip (embedded in layer 2) and with the microfluidic inlet and outlet included in layer 1. The thickness of layer 3 was initially set at 175 μm, although several thicknesses between 175 μm and 380 μm were evaluated in the optimization of the microfluidic flow cell performance. An image of the three layers assembled with the silicon chip is illustrated in Fig. 1B.

Both symmetrical structures were assembled with the microelectrodes of the two chips facing each other, and incorporating a porous membrane (25 μm thickness, 55% porosity, and 0.21 μm × 0.05 μm pores, Celgard 2500, Celgard, Charlotte, NC, USA) between both microchannels. The symmetrical structures were clamped with six 3-mm diameter screws to avoid fluidic leakage (Fig. 1C). Fig. 1D shows an image of the final microfluidic flow cell. In the characterization of the microfluidic flow cell, the solutions were inoculated into the system with two 5 mL syringes connected to two external syringe pumps (Nemesys B101-02B, Cetoni GmbH, Korbussen, Germany).

2.4. Computational simulations

The effect of the variation of the main design parameters involved in the performance of the microfluidic flow cell was evaluated by using the computational COMSOL Multiphysics® 6.0 software (from now referred as COMSOL). In all the cases, a Tertiary Current Distribution (Nernst-Planck Interface) was used as the physics interface to carry out the simulations. This interface enabled to simulate the potential distribution of the electrochemical cell by considering the transport of the ions and other phenomena as diffusion, convection or migration transport of uncharged species, by considering the Nernst-Planck equation.

A 2D design of the microfluidic flow cell was employed for the simulations aiming to generate a model able to predict the kinetics and final concentration of KTP extracted in ammonium buffered solution. The simulations considered the following conditions and extraction mechanism: (i) a 10 mM ammonium buffer water solution at pH 10.5 with KTP (donor solution) and a 10 mM ammonium buffer water solution at pH 10.5 without KTP (acceptor solution), were inoculated through the inlets of the microfluidic flow cell placed on the top layer, as is schematised in Fig. 2A; (ii) The KTP was spontaneously dissociated in the donor solution, forming negative charged ions; (iii) The positive potential applied between the microelectrodes in both sides of the microchannel induced the migration of negatively-charged KTP molecules through the 25 μm-thick membrane doped with 1-octanol, from the donor to the acceptor phase solution; and (iv) the microextraction efficiency was determined by comparing the quantity of the KTP present in the outlet of the acceptor solution, with the quantity of the KTP inoculated in the inlet of the donor solution.

Different microelectrode configurations and working conditions were evaluated using COMSOL and compared in terms of microextraction efficiency percentage. The extraction efficiency was defined as the percentage of KTP in the outlet of the acceptor solution in relation to that present in the inlet of the donor solution (microextraction efficiency = (KTP concentration in the acceptor solution outlet / KTP concentration in the donor solution inlet) × 100). And the microextraction efficiency percent variation was defined as the difference between the efficiency of one case of study versus the first case, divided by the value obtained in the first case, in percentage terms. The influence in the microextraction efficiency of the applied potential, the flow rate, the thickness of the microfluidic channels, the total area and positioning of the microelectrodes was evaluated (details of the microelectrodes in Fig. 2B). An initial KTP concentration in the inlet of the donor solution of 3 ppm was considered in all simulations.

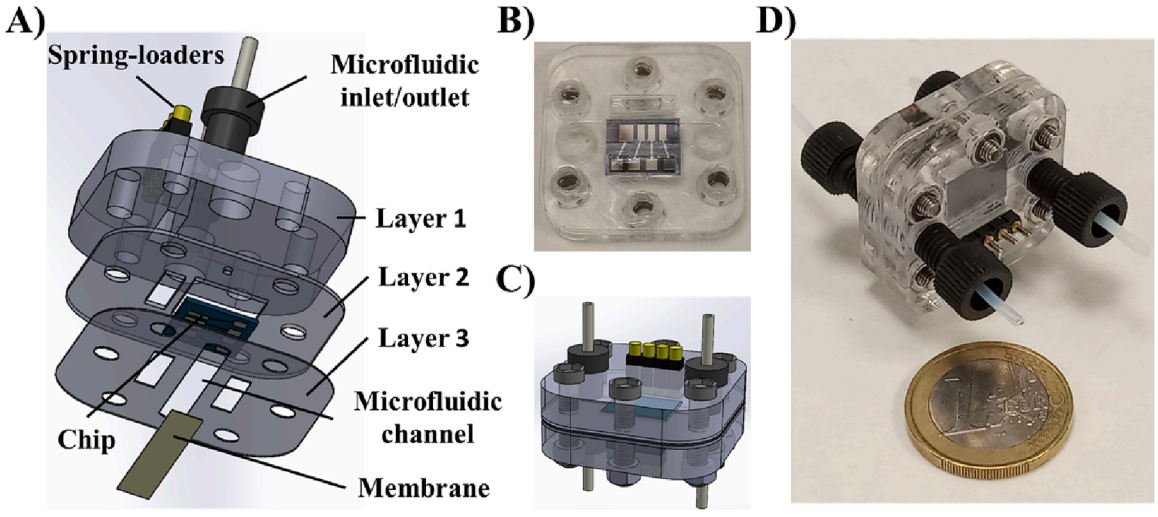

Fig. 1. A) Schematic layer by layer view of one of the parts of the microfluidic flow cell; B) Detailed image of the bonded three layers forming one of the parts of the microfluidic device; C) Schematic view of both parts assembled; D) Detailed image of the microfluidic flow cell.

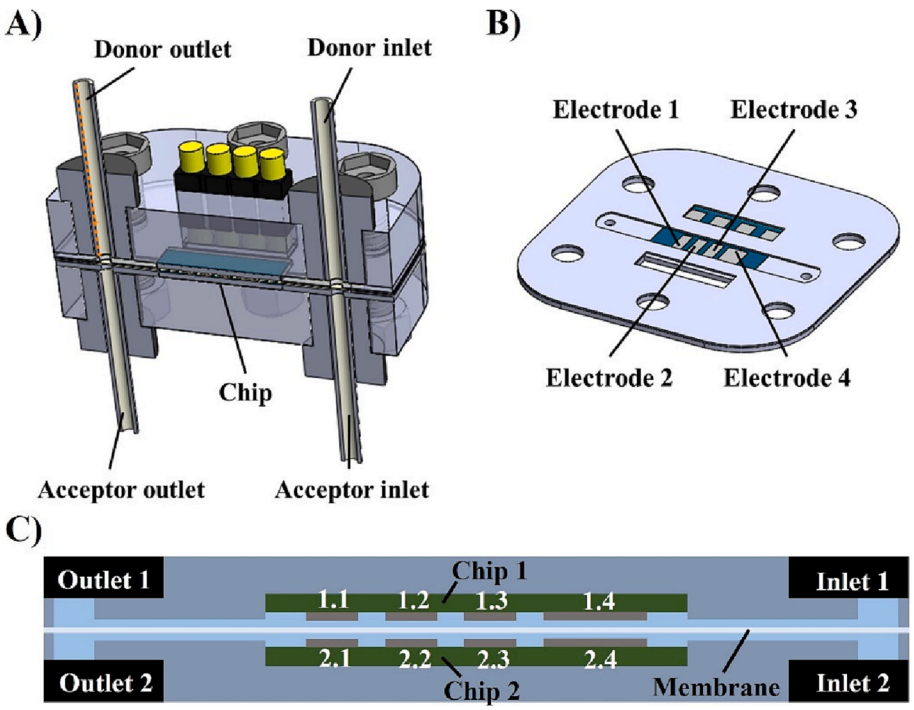

Fig. 2. A) 3-D scheme of the microfluidic flow cell cross section; B) Detailed scheme detailing the position and the 3-D view of the layers 2 and 3 including the chip and the microchannel; C) Cross-section of the microfluidic performance of the microfluidic flow cell.

In COMSOL simulations, the theoretical model and the microelectrodes labelling presented in Fig. 2C were employed. The influence in the microextraction efficiency of the applied potential, the flow rate and the microchannels thickness were evaluated with the same model, varying the parameter under study, while keeping constant the other two. In all cases, the microextraction potential was applied between the microelectrodes 2.4, 2.3 and 2.2 in the acceptor and the microelectrodes 1.4, 1.3 and 1.2 in the donor phase. This ensured a high microelectrode area for the microextraction process (three microelectrodes from each chip), while leaving one of the microelectrodes of each chip free (microelectrodes 2.1 and 1.1) for the EIS chemical analysis between the electro-membrane.

The position and total area of the microelectrodes used to apply the microextraction potential was also studied in detail to quantify their influence in the microextraction efficiency percent variation. The following combinations of microelectrodes (according to the scheme in Fig. 2C) were tested: (i) the 2.4 + 2.3 + 2.2 and the 1.4 + 1.3 + 1.2; (ii) the 2.4 + 2.3 and the 1.4 + 1.3; (iii) the 2.4 and the 1.4; (iv) the 2.4 and the 1.3; (v) the 2.4 and the 1.2; (vi) the 2.3 and the 1.4; (vii) the 2.3 and the 1.3; (viii) the 2.3 and the 1.2; (ix) the 2.2 and the 1.4; (x) the 2.2 and the 1.3; (xi) the 2.2 and the 1.2. In this study, the flow rate, the potential and the microchannels thickness were kept constant during all the simulations.

2.5. Validation of the simulation studies

The influence of the conditions from the COMSOL simulations were also experimentally validated by a series of assays of microextraction with the manufactured microanalytical flow cell. The process was as follows: (i) the porous membrane was doped with 1-octanol and allocated between both microfluidic channels placed in each of the polymeric structures of the microfluidic flow cell as is detailed in Fig. 1A; (ii) the two symmetrical structures forming the microfluidic flow cell were assembled by using the screws; (iii) both the acceptor (10 mM ammonium buffer solution at pH 10.5) and the donor solution (10 mM ammonium buffer solution at pH 10.5 containing KTP) were flowed inside the microchannels by using the fluidic inlets; (iv) a potential was applied between the microelectrodes placed in both microchannels to extract the KTP from the donor to the acceptor solution through the electro-membrane; and (vi) 12-μL extracts were collected in the outlet of the acceptor solution after the microextraction process to determine by HPLC-DAD the microextraction efficiency (as is described in Section "Chromatographic measurements").

The influence of the extraction conditions was also evaluated in the experimental system, namely the microextraction potential (from + 3 V to + 7 V), the flow rate in the donor and acceptor microchannel (between 3 μL/min and 5 μL/min); the microchannel thickness (from 175 μm to 380 μm); and the microelectrodes configuration by varying the number (total area) and the position of the connected microelectrodes. During the evaluation of each experimental condition, the other parameters were kept constant.

2.6. Chemical analysis by impedance of the microfluidic flow cell

The microfluidic flow cell was calibrated with seven KTP concentrations by EIS analysis in the range from 0 ppm to 5 ppm to obtain the limit of detection (LOD), the sensibility, the reproducibility and the linear range for the chemical analysis of the molecule. A potential of + 7 V was applied between the microelectrodes placed in the acceptor (i.e., 2.2, 2.3 and 2.4) and the donor microchannels (i.e., 1.2, 1.3 and 1.4). Both the acceptor and the donor solution were injected at a flow rate of 3 μL/min. The acceptor extracts were collected for 4 min (total volume of 12 μL), measured by HPLC-DAD and compared with EIS data. EIS measurements were performed after the microextraction with the microelectrodes 1.1 (donor microchannel) and 2.1 (acceptor microchannel). EIS experimental conditions were as follows: Open Circuit Potential, OCP; 10 mV AC amplitude from 1 MHz to 10 Hz; 10 points per decade). During the EIS measurements, the potential and the flow rate were stopped to avoid interference in the impedimetric determination.

Finally, the influence of the microextraction time on the microextraction efficiency was studied in the range from 30 s to 180 s. The microextraction process was evaluated with the following conditions: +7 V, 175 μm-thick microchannels and 3 μL/min, using the microelectrodes 2.2 and 2.1 in the acceptor, and 1.2 and 1.1 in the donor

microchannel, respectively, and with the donor solution initially containing 1 ppm of KTP. EIS measurements were performed at previous experimental conditions (i.e., OCP; 10 mV AC amplitude from 1 MHz to 10 Hz; 10 points per decade) by using two different microelectrodes configurations: (i) 1.1 (donor microchannel) vs. 2.1 (acceptor microchannel) to analyse the impedance in the electro-membrane; (ii) and 2.1 (acceptor microchannel) vs. 2.2 (acceptor microchannel) to monitor the changes in the acceptor phase. As before, 12 μL of the acceptor solution were collected and measured by HPLC-DAD to calculate the microextraction efficiency.

2.7. Chromatographic measurements

The HPLC-DAD was used as the golden standard to validate all the experimental assays described before. Briefly, 5 μL extracts were measured by using a mobile phase consisting of 0.1% formic acid at pH 2.6 (component A) and methanol (component B). The isocratic method was performed with 30% component B for 5 min, at a flow rate of 0.5 mL/min and at 25 °C. The KTP wavelength used for the diode-array detection (DAD) was 255 nm, with a retention time of 4.8 min. Consecutive extracts were injected after 3 min to properly re-equilibrate the column to the initial conditions.

The microextraction efficiency (EE) for KTP in the HPLC-DAD was calculated according to the following equation (eq. (1)):

$$EE = \frac{n_a}{n_0} x100\% = \frac{V_a C_a}{V_o C_o} x100 \quad (1)$$

Where, n_a is the number of moles found in the acceptor phase, n_o is the number of initial moles in the donor phase. V_a and V_o are the volumes used for the acceptor and the donor phase, respectively. C_a is the concentration of the KTP in the outlet of the acceptor solution and C_o is the initial concentration of the KTP in the inlet of the donor solution.

3. Results and discussion

3.1. Computational validation

The influence of the microextraction conditions in the designed microfluidic flow cell were firstly simulated with COMSOL. A 2-dimensional model approximation of the microfluidic flow cell was used to reduce the complexity of the calculations, and therefore the simulation time (Figure S1, in the Supplementary Information -SI-). It is important to highlight that the tertiary current distribution physics used in the simulations enabled to define the parameter "out-of-plane thickness". This parameter defined the thickness of the geometry perpendicular to the two-dimensional cross-section (microchannel thickness), instead of being a 2-dimensional model. The following parameters were defined and set constant along all the simulations: diffusion coefficients for NH_4^+ and Cl^- of 1.0×10^{-9} m^2/s; 298.5 K of temperature; NH_4Cl concentration in the inlet of 0.05 mol/dm^3; cell length of 0.0068 m; membrane width of 0.025 mm; microchannel thickness (out-of-plane thickness) of 2.5 mm; and KTP concentration in the inlet of 1.2×10^{-5} mol/dm^3. Regarding the tertiary current distribution definition, best results were obtained considering: (i) a mass transport of the dissolved species based on both diffusion and migration effects; (ii) water-based with electroneutrality as the charge conservation model; and (iii) three species as dependent variables (NH_4^+ and Cl^- from the buffer and KTP^- from the analyte).

The following assumptions were considered in the simulations. First, the general mass balance for the diluted species in the electrolytes was defined by the following equation (eq. (2)):

$$dc_i/dt + \nabla \times N_i = R_{i,tot} \quad (2)$$

The equation was directly proportional to the total flow of the species in the electrolyte (N), which is defined by the Nernst-Planck equation (eq. (3)):

$$N_i = -D_i \nabla c_i - z_i u_{m,i} F c_i \nabla \varnothing_l + c_i u = J_i + c_i u \quad (3)$$

which depends on the concentration (c_i), the valence (z_i), the ion coefficient of diffusion (D_i) and the mobility ($u_{m,\ i}$) of the ion, the Faraday constant (F), the electrolyte potential ($\varnothing_l$), the velocity (u) and the molar flow related to the convective transport (J_i).

The mass transport considered the transport of mass from the donor to the acceptor microchannel by diffusion and migration. The diffusion, corresponding to the spontaneous transport of diluted species from the microchannel with a higher concentration to that with a lower one, considered only the mass transfer coefficient to simplify the calculations [31]. Only small changes of concentration near the microchannels and the membrane interfaces were assumed.

The migration considered the movement of charged particles in the generated electric field, and they were based on the Nernst-Einstein equation (eq. (4):

$$u_{m,i} = Di/RT \quad (4)$$

The migration was directly proportional to the D_i, dependent on the electric field gradient applied between the microelectrodes in both sides of the membrane, and inversely proportional to the Planck constant (R) and the temperature (T).

The water-based electrolyte charge conservation considered the proton and hydroxyl transport from water ionisation automatically in the computational model. Therefore, the initial pH value in the simulation only depended on the concentration of the previously defined constant species. Regarding the ion exchange membrane, the same mass transport mechanisms were considered with minimal modifications. Concretely, the coefficient of diffusion of the species though the membrane was adjusted (1.0×10^{-9} m^2/s for both the NH_4^+ and the Cl^- ions, 8.0×10^{-10} m^2/s for the KTP^-, 9.3×10^{-9} m^2/s for the H^+, and 5.3×10^{-9} m^2/s for the OH^-) according to bibliography [32], and the electrolyte volume fraction (ε), which is related to the membrane porosity (porous matrix properties − 25 μm thickness, 55% porosity, and 0.21 μm × 0.05 μm pores -), was set at a value of 0.41. A free-triangular user-controller mesh, with an element size normal calibrated for fluid dynamics (maximum element size of 0.0169 mm, minimum element size of 7.5×10^{-4} mm, maximum element growth rate of 1.15, curvature factor of 0.3 and resolution of narrow regions of 1) was selected for the simulations. Finally, a stationary study model as solver was applied to compute the study flow and the chemical composition at the equilibrium for the chemical species.

A general view of the results obtained from the simulations are shown in Figure S1 (in the SI). Figure S1A (in the SI) represents the electrolyte potential distribution generated in the microfluidic flow cell after the application of a + 7 V potential between the microelectrodes 1.4, 1.3 and 1.2 (acceptor microchannel) and the microelectrodes 2.4, 2.3 and 2.2 (donor microchannel). The surface colour and the grey lines represent the electrolyte potential and the electrolyte density current vectors generated throughout the microfluidic flow cell, respectively. Simulation results showed high electrolyte potentials (red colour corresponding to + 7 V) on the acceptor microelectrodes applying the positive potential and low electrolyte potential (dark blue colour) on the donor microelectrodes. Intermediate areas between both microelectrodes presented potentials between + 2 V and + 6 V, with increasing values when approaching to the acceptor microelectrodes, as was expected. Regarding to the electrolyte current density vectors, which were described as the sum of fluxes of all the ions in the electrolyte, perpendicular vectors meaned that the current density was maximum along the surface of the face-to-face microelectrodes applying the microextraction potential. Curved vectors in the microchannels areas without microelectrodes also demonstrated the existence of an ions flow along the microchannel during microextraction process. This potential and current density distribution favoured the migration of negatively-charged KTP ions in ammonium buffer from the donor (initial KTP

concentration = 3 ppm) to the acceptor solution (initial KTP concentration = 0 ppm). The distribution of the KTP ions throughout the microchannels is illustrated in Figure S1B (in the SI). Red-coloured areas corresponded to high KTP concentration (3 ppm), and blue-coloured areas to a KTP concentration of 0 ppm. Intermediate values of KTP concentration were represented with different colours, where warmer ones corresponded to higher KTP concentrations.

A small KTP concentration (blue colour) was found close to the acceptor inlet since mass transport at this point was mainly dependent on diffusion. Higher KTP concentrations were observed along the acceptor microchannel, with warmer colours closer to the outlet. The result confirmed that mass transport was dominated by migration in response to the electric field gradient generated between the microelectrodes. This validated the suitability of the design and the microfluidic flow cell model to study microextraction processes.

3.1.1. Effect of the applied potential.

The influence of several key parameters in the microextraction efficiency was studied, concretely the applied potential, the flow rate, the microchannels thickness and the number and position of the microelectrodes, as described in Section 2.4. As shown in Figure S2A (in the SI), it was a direct correlation between the applied potential and the microextraction efficiency. These results were in agreement with the Nernst-Planck equation, where the flow of charged species is linearly related to the potential in the electrolyte. According to that, the microextraction potential should be as high as possible, but avoiding electrolysis and other problems associated to the use of large potentials.

3.1.2. Effect of the flow rate.

The microextraction efficiency decreased with the flow rate (Figure S2B, in the SI), as was expected from the Nernst-Einstein equation. According to that equation, in migration-dominated systems the migration depends linearly on the microextraction time (i.e., residence time of the species in a fluidic system). Therefore, the flow rate should be kept as small as possible to guarantee a high microextraction efficiencies. When comparing the influence of both parameters in the microextraction of charged molecules, it was evident that the influence of the potential rate was higher than the flow rate, since the slope of the linear trendline of the former was 27 % higher than the latter.

3.1.3. Effect of the microchannels thickness.

The variation in the microextraction efficiency with the microchannels thickness is illustrated in Figure S2C (in the SI), which presenting a polynomial decay. This behaviour was in agreement with the second term of the Nernst–Planck equation (see eq. (3), in which $\nabla \varnothing_l$ is inversely proportional to the distance between microelectrodes [33]. Therefore, this parameter was found to be the most critical one since small changes in thickness resulted in a large variation in microextraction efficiency.

3.1.4. Effect of the number of electrodes.

Finally, the influence of the number (total area) and the position of the microelectrodes in the microextraction was also studied. Results are illustrated in Figure S2D (in the SI), where the plot in the left shows the effect of the total area of the microelectrodes in the microextraction process and the one in the right the effect of the electrode position. A linear correlation was observed between the total area magnitude and the microextraction efficiency, as expected when considering migration processes in microfluidic systems operating at constant flow. The microelectrodes position also influenced the microextraction efficiency. Configurations with the microelectrodes in both microchannels faced each other (configuration vii -electrodes 2.3 and configuration 1.3- and xi -electrodes 2.2 and 1.2-) presented lower microextraction efficiencies than the others. The increasing of the microextraction efficiency when an electrode in one channel is displaced relative to an electrode on the other channel was related to the increase of the current density vectors and the ionic migration associated to it.

As a summary, and considering all the computational simulations, the microfluidic flow cell should obtain high microextraction efficiencies by applying high microextraction potentials in microelectrode arrays facing each other with a high total area, and by using low flow rates and thin microchannels. The configuration corresponding to a three-microelectrodes facing each other was considered the best architecture for efficient microextraction with the microanalytical flow cell.

3.2. Experimental microextraction results with the microfluidic flow cell

Computational simulations were validated experimentally with the microextraction system implemented in the set-up illustrated in Fig. 3A by applying the experimental conditions detailed in the section 2.6. Both the donor and the acceptor solutions were flowed from the right (inlets) to the left (outlets) side of the microfluidic flow cell, as it is shown in Fig. 3B. The microextraction efficiency was studied at: (i) microextraction potentials in the range from + 3 V to + 7 V (Fig. 5C); (ii) flow rates between 3 μL/min and 5 μL/min (Fig. 5D); (iii) microchannel thicknesses in the range from 175 μm to 380 μm (Fig. 5E); and (iv) different microelectrodes configurations (Fig. 5F). In agreement with computational simulations, higher microextraction efficiencies were obtained when applying high microextraction potentials (+7 V) in a configuration involving large microelectrode areas of microelectrodes facing each other (microelectrodes configuration i in Fig. 5F), low flow rates (3 μL/min) and thin microchannels (175 μm). The low microextraction efficiency obtained of 43% at optimal conditions may be associated with some limitations of the experimental set-up. Concretely, the applied potential could not be increased over + 7 V because of damage of the metallic surface and electrolytic corrosion; the flow rate could not be decreased below 3 μL/min for the high pressures generated in the microchannels during the assays; the microchannel thickness could not be reduced below 175 μm for the lack of available manufacturing systems; the location, the area and the number of electrodes could not be modified since dependant on the chip design. Despite of these experimental limitations, the reproducibility and repeatability of the microextraction process was very high (three different systems were used for of each studied condition were used the same day, obtaining a relative standard deviation lower than 5%), demonstrating the potential of the proposed microfluidic flow cell for an accurate microextraction. In the next assays, the conditions providing the optimal microextraction efficiencies were employed to fully validate the presented microanalytical flow system for simultaneous microextraction and chemical analysis.

3.3. Analytical assessment of the microfluidic flow cell

The analytical capacities of the microfluidic flow cell for the detection of KTP were evaluated under optimal microextraction conditions in presence of seven concentrations of KTP (i.e., 0.3 ppm, 0.5 ppm, 1.0 ppm, 2.0 ppm, 3.0 ppm, 4.0 ppm and 5-0.0 ppm). The relationship between the KTP concentration in the analytical solution and the impedimetric signal was determined in situ as follows (see Fig. 4A): (1) the donor and the acceptor solutions were flowed at 3 μL/min for 3 min to properly fill the microchannels with the solutions; (2) then, a + 7 V microextraction potential was applied between the microelectrodes in the acceptor (microelectrodes 2.2 + 2.3 + 2.4) and the donor (microelectrodes 1.2 + 1.3 + 1.4) microchannels during 4 min; and (3) after the microextraction process, impedance measurements were performed between the microelectrodes 1.1 (donor) and 2.1 (acceptor) to correlate the recorded signal with the KTP concentration in the solution. Based on a previous publication of the group [27], the equivalent circuit presented in the Fig. 4B was used to characterize the proposed microanalytical flow system. The circuit consisted of four components: the resistance of the electrolyte solution (R_S), the double layer capacitance (C_{dl}) -here represented by a constant phase element to consider the

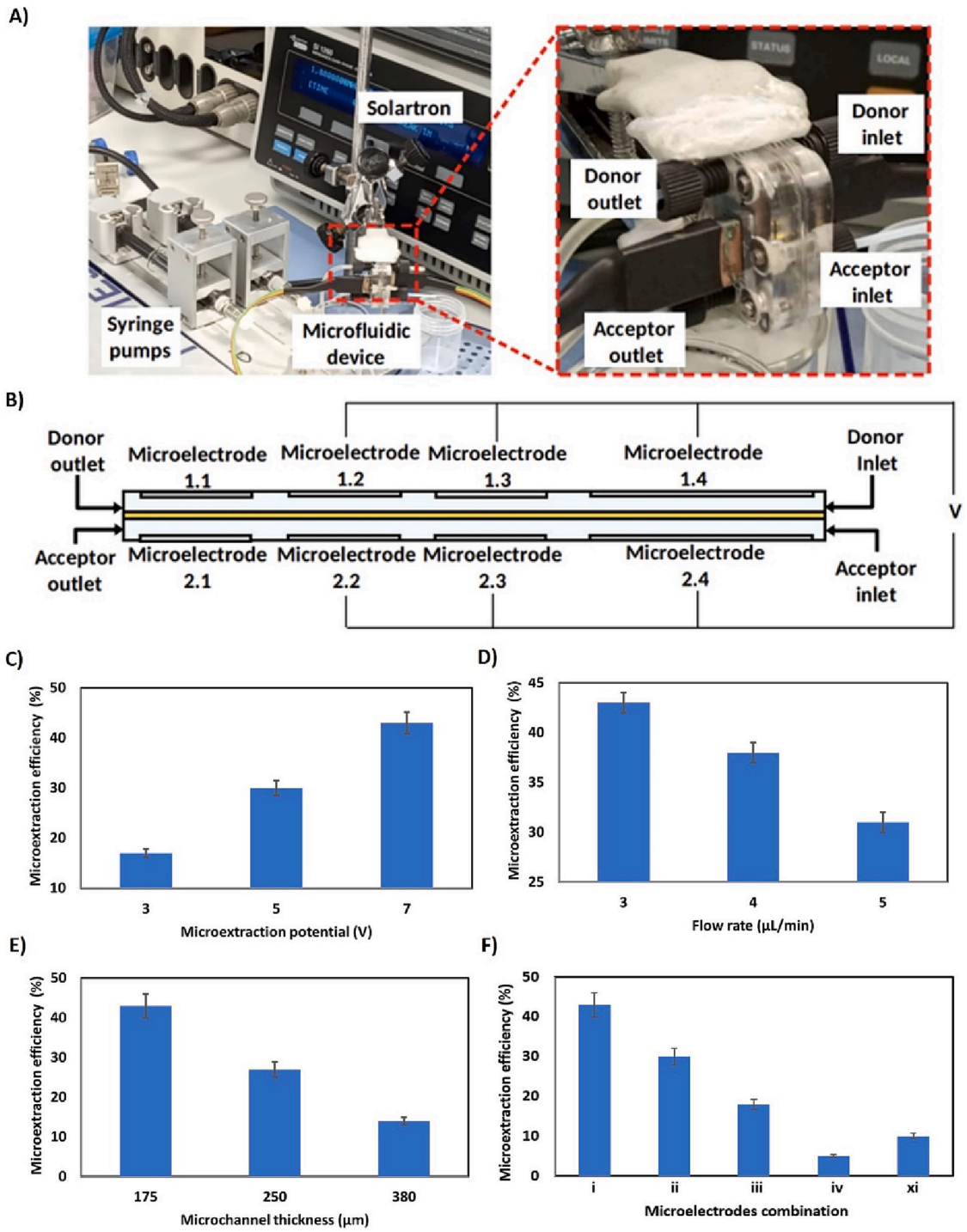

Fig. 3. A) Image of the set-up used during the experimental measurements with the microfluidic flow cell; B) Scheme of the experimental procedure followed to carry out the assays; C) Experimental microextraction efficiencies obtained for a potential of + 3 V, +5 V and + 7 V; D) Experimental microextraction efficiencies obtained for a flow rate of 5 µL/min, 4 µL/min and 3 µL/min; E) Experimental microextraction efficiencies obtained for a microchannels thickness of 175 µm, 250 µm and 380 µm; F) Experimental microextraction efficiencies obtained for different combinations of microelectrodes: (i) 1.2 + 1.3 + 1.4 + 2.2 + 2.3 + 2.4; (ii) 1.3 + 1.4 + 2.3 + 2.4; (iii) 1.4 + 2.4; (iv) 1.3 + 2.4; and (xi) 1.2 + 2.2. Each bar represents the mean efficiency percentage value of three replicates recorded consecutively under the same conditions, with the error bars being the corresponding standard deviation.

roughness of the microelectrode surface-, the capacitance of the membrane (C_M) and the resistance of the membrane (R_M). The R_M was experimentally determined (see Figure S3, in the SI) as the diameter of the semicircle of the plot from the Nyquist diagram for each concentration of KTP in the solution (Fig. 4C). As can be seen in Fig. 4C, the diameter of the semicircle decreased (and therefore the resistance of the membrane) when increasing the KTP concentration, following an inversely proportional linear correlation in the range between 0.5 ppm and 5.0 ppm. The lowest KTP concentration (0.3 ppm) showed a high R_M value in comparison to the other concentrations which does not fall within the linear adjustment, meaning that the resistance of the membrane for concentrations below 0.5 ppm of KTP is very high and the flux of the ions is not as favoured as for higher KTP concentrations. The sensitivity of the measurement was −11120.7 ± 778.5 Ω/ppm

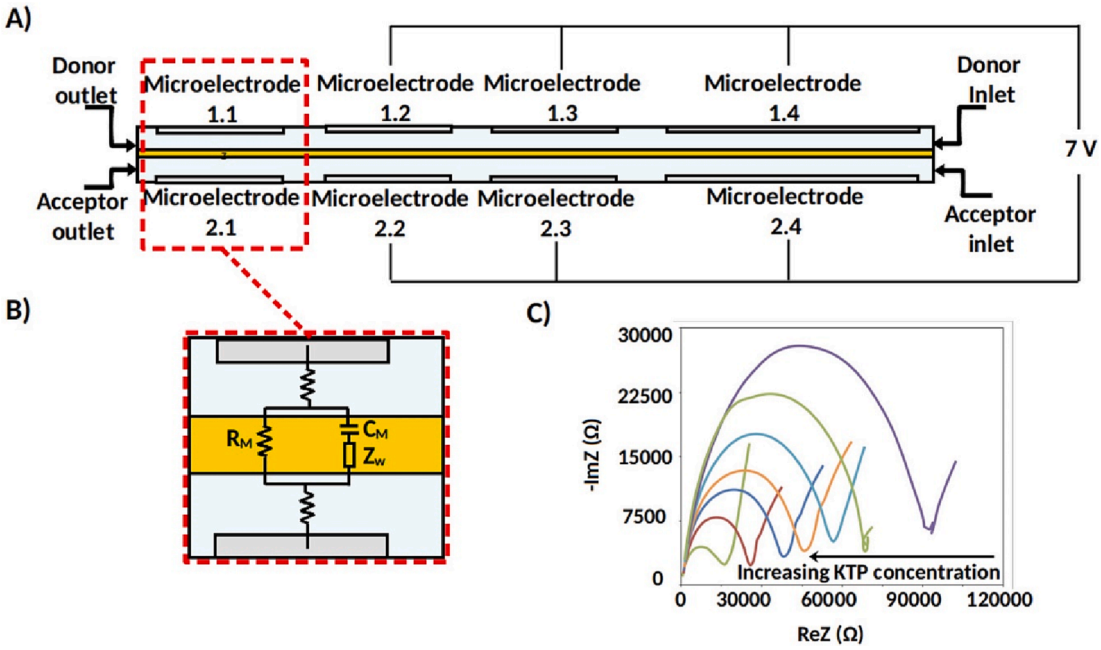

Fig. 4. A) Scheme of the experimental procedure and the electrical connections to carry out the impedimetric tests; B) Equivalent circuit of the impedance spectra; C) Nyquist plots for different KTP concentrations.

(coefficient of correlation -R^2- = 0.996), with a LOD (calculated using the 3σ IUPAC criterion and the lowest concentration distinguishable from zero −0.3 ppm-) of 0.12 ± 0.01 ppm (Figure S4, in the SI), and a relative standard deviation (R.S.D.) of the sensitivity lower than 4% (n = 3).

Impedimetric detection of KTP considered the change in the medium conductivity (i.e., Rs) associated to the presence of charged KTP concentration. The simplicity and rapidness of the impedance measurement allowed continuous KTP detection and was used to monitor microextraction efficiency in real time. The real time analysis of microextraction is presented in Fig. 5A, while the two microelectrode configurations used in the impedance measurements is schematized in Fig. 5B. Experimentally, two electrode configurations were employed for impedance analysis, namely (i) two faced microelectrodes located in different microchannels (1.1 + 1.2 and 2.1 + 2.2, corresponding to the microelectrodes combination ii) and (ii) two serial microelectrodes both located in the acceptor microchannel (2.1 + 2.2) for precise analysis of Rs in the acceptor phase. To study the microextraction efficiency of a 1 ppm KTP solution over time, a + 7 V microextraction potential was applied in the system during different times between 0 s and 180 s (0 s, 30 s, 60 s, 90 s, 120 s and 180 s). The acceptor solution (9 μL) was collected after each microextraction to be analysed by HPLC-DAD for comparison with impedance data. Between consecutive measurements, the system was totally cleaned by flowing fresh solutions in both the acceptor and the donor microchannels. The aim of this assay was to determine the optimal microextraction time by monitoring microextraction efficiency in real time. Results showed important differences between the impedimetric response of both microelectrode configurations. In the case of faced microelectrodes, R_M presented similar magnitudes over time (Fig. 5C), whereas a clear decrease in resistance was obtained when employing only microelectrodes in the acceptor microchannel (Fig. 5D). There was a clear correlation between impedance data from the second configuration (serial microelectrodes in the acceptor microchannel) and chromatographic measurements, which presented a linear increase of the microextraction efficiency for the 1 ppm KTP solution with the microextraction time (Fig. 5E). The value of the microextraction efficiency (around 30%) also correlates with the obtained in the section 3.2 for the same microelectrodes configuration and conditions (see Fig. 3F, microelectrodes combination ii), demonstrating again the high reproducibility of the system.

These results demonstrates that the proposed microfluidic flow cell could be used to properly monitor on time the amount of the KTP extracted from the donor through impedance measurement, as well as the quantification of KTP extracts of unknow concentration by interpolation in the calibration curve thanks to the high repeatability of the measurement system. This confirmed that the proposed proof of concept microanalytical flow system could be used for both analytes microextraction and analysis, avoiding the need for sample collection and transport to the laboratory for analysis with standard methods (HPLC-DAD) and the associated costs.

4. Conclusions

A proof of concept of a new microfluidic platform integrating microelectrodes and an EME-based microextraction process in a fast prototyped microfluidic flow cell has been studied and validated by using EIS. Two silicon chips with 4 platinum microelectrodes placed on both sides of the doped membrane enable, for the very first time, the simultaneous monitoring of the microextraction process and the full chemical characterization of the system by using impedance technique.

Although some microfluidic systems in the literature have allowed their on-line coupling to analysis instruments (e.g., HPLC-DAD), they entail a great analysis time and hinder their portability. These challenges have been addressed with the promising operational results of the developed compact microfluidic flow cell. The performed on-time microextraction and EIS characterization of KTP in this work drastically reduces the sample consumption and the microextraction times of analytes in comparison to current methods, resulting in a perfect candidate with unique characteristics to develop the next generation of on-site and remote analytical control systems.

The presented proof of concept platform presented here could be applied to analytes of different chemical nature and from different matrices, by adapting the design and using more advanced and reliable manufacturing processes for increasing the extraction efficiency and improving the limit of quantification, meaning that its applicability can be broaden to environmental, biological or pharmaceutical analysis.

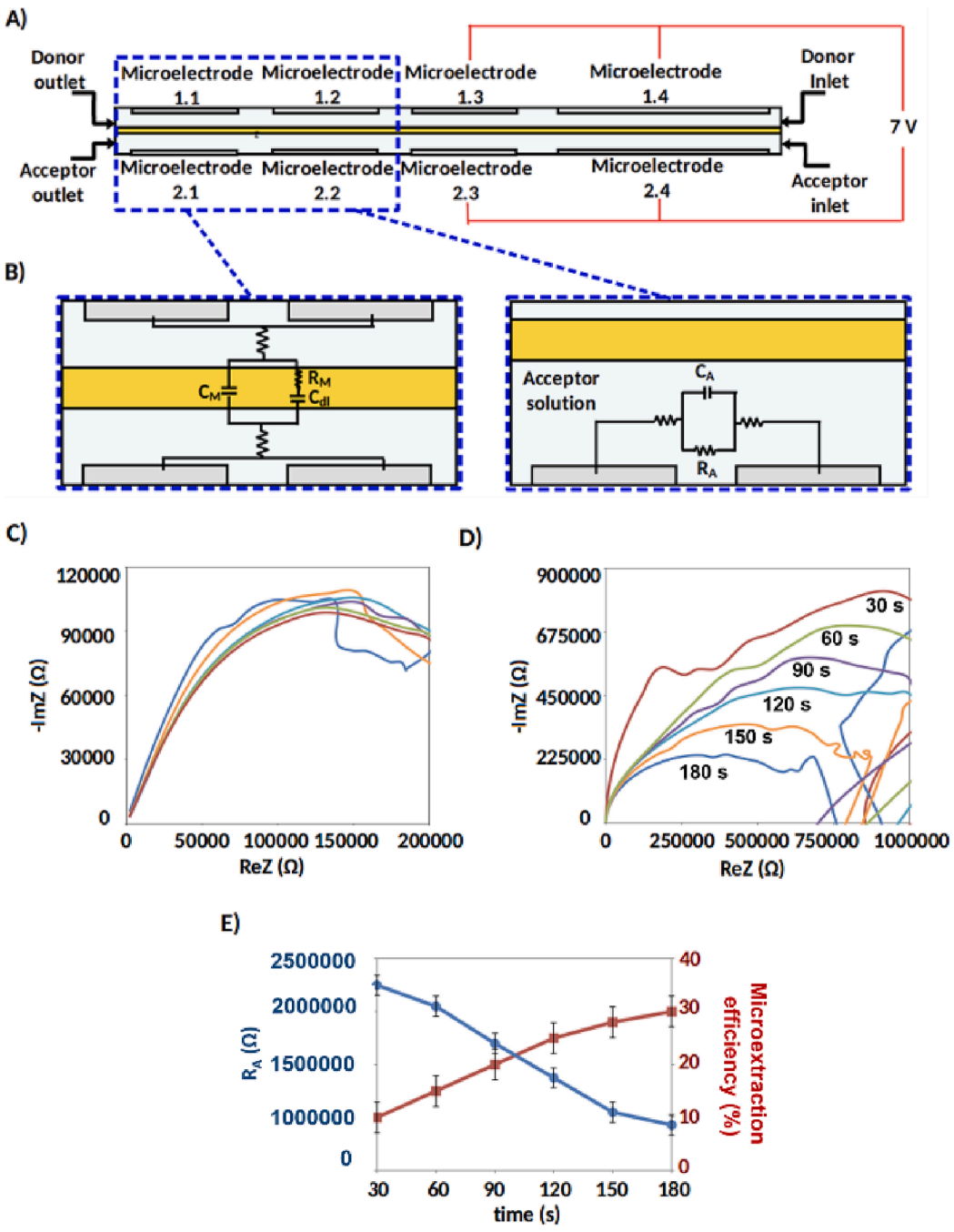

Fig. 5. A) Scheme of the experimental procedure and the electrical connections to carry out the impedimetric tests of the microextraction tests over time; B) Equivalent circuit of the impedance spectra when the microelectrodes 1.1 and 2.1 (left scheme) and the microelectrodes 2.1 and 2.2 (right scheme) are used; C) Nyquist plots for different microextraction times obtained from the micro microelectrodes 1.1 and 2.1; D) Nyquist plots for different microextraction times obtained from the microelectrodes 2.1 and 2.2. Arabic numbers represent the extraction time corresponding to each recorded plot; E) In red colour, the evolution curve obtained from the Nyquist diagram for microelectrodes 2.1 and 2.2. Each point represents the mean RA value of three replicates recorded consecutively for each time, with the error bars being the corresponding standard deviation. In blue colour, the evolution curve of the experimental microextraction efficiency obtained by chromatography. Each point represents the mean percentage of the microextraction efficiency of three replicates recorded consecutively for each time, with the error bars being the corresponding standard deviation. (For interpretation of the references to colour in this figure legend, the reader is referred to the web version of this article.)

This is the first platform described in the literature with a real potential to be applied for in situ extraction and detection analysis. Future work will focus on the full portability of the developed proof-of-concept for decentralized analysis, replacing the electronic analyzer and syringe pumps used here with an integrated digital impedance analyzer and battery-powered electronic micropumps.

Declaration of Competing Interest

The authors declare that they have no known competing financial interests or personal relationships that could have appeared to influence the work reported in this paper.

Data availability

Data will be made available on request.

Acknowledgments

This work was financially supported by the Ministry of Science, Innovation and Universities - State Research Agency -AEI- and European Regional Development Fund -ERDF- (RTI2018-101974-B-C-21 and PID2021-127653NB-C21). E. Santigosa thanks Universitat Autònoma de Barcelona (UAB) for her PIF fellowship supported by the Agencia de Gestió d'Ajusts Universitaris i de Recerca (2017-SGR-329). A. Moreno is grateful to MICINN for the grant of a PhD studentship from the FPI program (PRE2019-088338).

Appendix A. Supplementary data

Supplementary data to this article can be found online at https://doi.org/10.1016/j.microc.2023.109044.

References

[1] H.A. Stone, A.D. Stroock, A. Ajdari, Engineering Flows in Small Devices: Microfluidics Toward a Lab-on-a-Chip, Engineering flows in small devices: Microfluidics toward a lab-on-a-chip 36 (1) (2004) 381–411.

[2] D. Mark, S. Haeberle, G. Roth, F.V. Stetten, R. Zengerle, Microfluidic lab-on-a-chip platforms: Requirements, characteristics and applications, Chem Soc Rev. 39 (2010) 1153–1182, https://doi.org/10.1039/b820557b.

[3] S. Haeberle, R. Zengerle, Microfluidic platforms for lab-on-a-chip applications, Lab Chip. 7 (2007) 1094–1110, https://doi.org/10.1039/b706364b.

[4] A. Sarafraz-Yazdi, A. Amiri, Liquid-phase microextraction, TrAC -, Trends in Analytical Chemistry. 29 (2010) 1–14, https://doi.org/10.1016/j.trac.2009.10.003.

[5] E. Carasek, G. Bernardi, S.N. do Carmo, C.M.S. Vieira, Alternative green extraction phases applied to microextraction techniques for organic compound determination, Separations. 6 (3) (2019) 35.

[6] C. Huang, Z. Chen, A. Gjelstad, S. Pedersen-Bjergaard, X. Shen, Electromembrane extraction, TrAC -, Trends in Analytical Chemistry. 95 (2017) 47–56, https://doi.org/10.1016/j.trac.2017.07.027.

[7] P. Gimenez-Gomez, R. Escude-Pujol, C. Jimenez-Jorquera, M. Gutierrez-Capitan, Multisensor Portable Meter for Environmental Applications, IEEE Sens J. 15 (2015) 6517–6523, https://doi.org/10.1109/JSEN.2015.2460011.

[8] D. Zhang, Q. Liu, Biosensors and bioelectronics on smartphone for portable biochemical detection, Biosens Bioelectron. 75 (2016) 273–284, https://doi.org/10.1016/j.bios.2015.08.037.

[9] A. Márquez, J. Aymerich, M. Dei, R. Rodríguez-Rodríguez, M. Vázquez-Carrera, J. Pizarro-Delgado, P. Giménez-Gómez, Á. Merlos, L. Terés, F. Serra-Graells, C. Jiménez-Jorquera, C. Domínguez, X. Muñoz-Berbel, Reconfigurable multiplexed point of Care System for monitoring type 1 diabetes patients, Biosens Bioelectron. 136 (2019) 38–46.

[10] A.F.D. Cruz, N. Norena, A. Kaushik, S. Bhansali, A low-cost miniaturized potentiostat for point-of-care diagnosis, Biosens Bioelectron. 62 (2014) 249–254, https://doi.org/10.1016/j.bios.2014.06.053.

[11] P. Cui, S. Wang, Application of microfluidic chip technology in pharmaceutical analysis: A review, J Pharm Anal. 9 (2019) 238–247, https://doi.org/10.1016/j.jpha.2018.12.001.

[12] M. Sonker, V. Sahore, A.T. Woolley, Recent advances in microfluidic sample preparation and separation techniques for molecular biomarker analysis: A critical review, Anal Chim Acta. 986 (2017) 1–11, https://doi.org/10.1016/j.aca.2017.07.043.

[13] A. Shahvar, D. Shamsaei, M. Saraji, N. Arab, S. Alijani, Microfluidic-based liquid-liquid microextraction in combination with smartphone-based on-chip detection for the determination of copper in biological, environmental, and food samples, Microchemical Journal. 160 (2021) 105655.

[14] K. Sato, M. Tokeshi, T. Sawada, T. Kitamori, Molecular transport between two phases in a microchannel, Analytical Sciences. 16 (2000) 455–456, https://doi.org/10.2116/analsci.16.455.

[15] N.J. Petersen, H. Jensen, S.H. Hansen, S.T. Foss, D. Snakenborg, S. Pedersen-Bjergaard, On-chip electro membrane extraction, Microfluid Nanofluidics. 9 (2010) 881–888, https://doi.org/10.1007/s10404-010-0603-6.

[16] M.D. Ramos Payán, H. Jensen, N.J. Petersen, S.H. Hansen, S. Pedersen-Bjergaard, Liquid-phase microextraction in a microfluidic-chip - High enrichment and sample clean-up from small sample volumes based on three-phase extraction, Anal Chim Acta. 735 (2012) 46–53, https://doi.org/10.1016/j.aca.2012.05.023.

[17] M. Ramos-Payan, S. Maspoch, A. Llobera, A simple and fast Double-Flow microfluidic device-based liquid-phase microextraction (DF-μLPME) for the determination of parabens in water samples, Talanta. 165 (2017) 496–501, https://doi.org/10.1016/j.talanta.2016.12.059.

[18] M. Karami, Y. Yamini, Y. Abdossalami Asl, M. Rezazadeh, On-chip pulsed electromembrane extraction as a new concept for analysis of biological fluids in a small device, J Chromatogr A. (1527 (2017)) 1–9, https://doi.org/10.1016/j.chroma.2017.10.049.

[19] M. Ramos-Payan, S. Maspoch, A. Llobera, An effective microfluidic based liquid-phase microextraction device (μLPME) for extraction of non-steroidal anti-inflammatory drugs from biological and environmental samples, Anal Chim Acta. 946 (2016) 56–63, https://doi.org/10.1016/j.aca.2016.09.040.

[20] Y.A. Asl, Y. Yamini, S. Seidi, M. Rezazadeh, Simultaneous extraction of acidic and basic drugs via on-chip electromembrane extraction, Anal Chim Acta. 937 (2016) 61–68, https://doi.org/10.1016/j.aca.2016.07.048.

[21] M. Ramos Payán, E. Santigosa, R. Fernández Torres, M.Á. Bello López, A New Microchip Design. A Versatile Combination of Electromembrane Extraction and Liquid-Phase Microextraction in a Single Chip Device, Anal Chem. 90 (2018) 10417–10424, https://doi.org/10.1021/acs.analchem.8b02292.

[22] F. Zarghampour, Y. Yamini, M. Baharfar, M. Faraji, Simultaneous extraction of acidic and basic drugs: Via on-chip electromembrane extraction using a single-compartment microfluidic device, Analyst. 144 (2019) 1159–1166, https://doi.org/10.1039/c8an01668b.

[23] E. Santigosa, S. Pedersen-Bjergaard, M. Muñoz, M. Ramos-Payán, Green microfluidic liquid-phase microextraction of polar and non-polar acids from urine, Anal Bioanal Chem. 413 (2021) 3717–3723, https://doi.org/10.1007/s00216-021-03320-9.

[24] C. Huang, K.F. Seip, A. Gjelstad, S. Pedersen-Bjergaard, Electromembrane extraction of polar basic drugs from plasma with pure bis(2-ethylhexyl) phosphite as supported liquid membrane, Anal Chim Acta. 934 (2016) 80–87, https://doi.org/10.1016/j.aca.2016.06.002.

[25] M.S. Restan, H. Jensen, X. Shen, C. Huang, Ø.G. Martinsen, P. Kubáň, A. Gjelstad, S. Pedersen-Bjergaard, Comprehensive study of buffer systems and local pH effects in electromembrane extraction, Anal Chim Acta. 984 (2017) 116–123, https://doi.org/10.1016/j.aca.2017.06.049.

[26] S.S. Nasrollahi, S.S.H. Davarani, H.R. Moazami, Impedometric investigation of salt effects on electromembrane extraction: Practical hints for pH adjustment, Electrochim Acta. 296 (2019) 355–363, https://doi.org/10.1016/j.electacta.2018.11.037.

[27] E. Santigosa-Murillo, X. Muñoz-Berbel, S. Maspoch, M. Muñoz, M. Ramos-Payán, Impedance model for voltage optimization of parabens extraction in an electromembrane millifluidic device, J Chromatogr A. 1625 (2020) 461270.

[28] G.D. Alkimin, A.M.V.M. Soares, C. Barata, B. Nunes, Evaluation of ketoprofen toxicity in two freshwater species: Effects on biochemical, physiological and population endpoints, Environmental Pollution. 265 (2020) 114993.

[29] J.K. Gierse, C.M. Koboldt, M.C. Walker, K. Seibert, P.C. Isakson, Kinetic basis for selective inhibition of cyclo-oxygenases, Biochemical Journal. 339 (3) (1999) 607–614.

[30] P. Giménez-Gómez, M. Gutiérrez-Capitán, F. Capdevila, A. Puig-Pujol, C. Jiménez-Jorquera, C. Fernández-Sánchez, Compact analytical flow system for the simultaneous determination of l-lactic and l-malic in red wines, Sci Rep. 10 (2020), https://doi.org/10.1038/s41598-020-76502-7.

[31] M.P. di Cagno, F. Clarelli, J. Vabenø, C. Lesley, S.D. Rahman, J. Cauzzo, E. Franceschinis, N. Realdon, P.C. Stein, Experimental Determination of Drug Diffusion Coefficients in Unstirred Aqueous Environments by Temporally Resolved Concentration Measurements, Mol Pharm. 15 (2018) 1488–1494, https://doi.org/10.1021/acs.molpharmaceut.7b01053.

[32] F. Lagrange, F. Pehourcq, B. Bannwarth, J.J. Leng, M.C. Saux, Passage of S-(+)- and R-(-)-ketoprofen across the human isolated perfused placenta, Fundam Clin Pharmacol. 12 (1998) 286–291, https://doi.org/10.1111/j.1472-8206.1998.tb00956.x.

[33] K. Krabbenhøft, J. Krabbenhøft, Application of the Poisson-Nernst-Planck equations to the migration test, Cem Concr Res. 38 (2008) 77–88, https://doi.org/10.1016/j.cemconres.2007.08.006.